Electronic Supplementary Information (ESI) for

A First Jump of Microgel; Actuation Speed Enhancement by Elastic Instability

Howon Lee, Chunguang Xia and Nicholas X. Fang*

Department of Mechanical Science and Engineering

University of Illinois at Urbana-Champaign, Urbana, IL, USA

E-mail: nicfang@illinois.edu

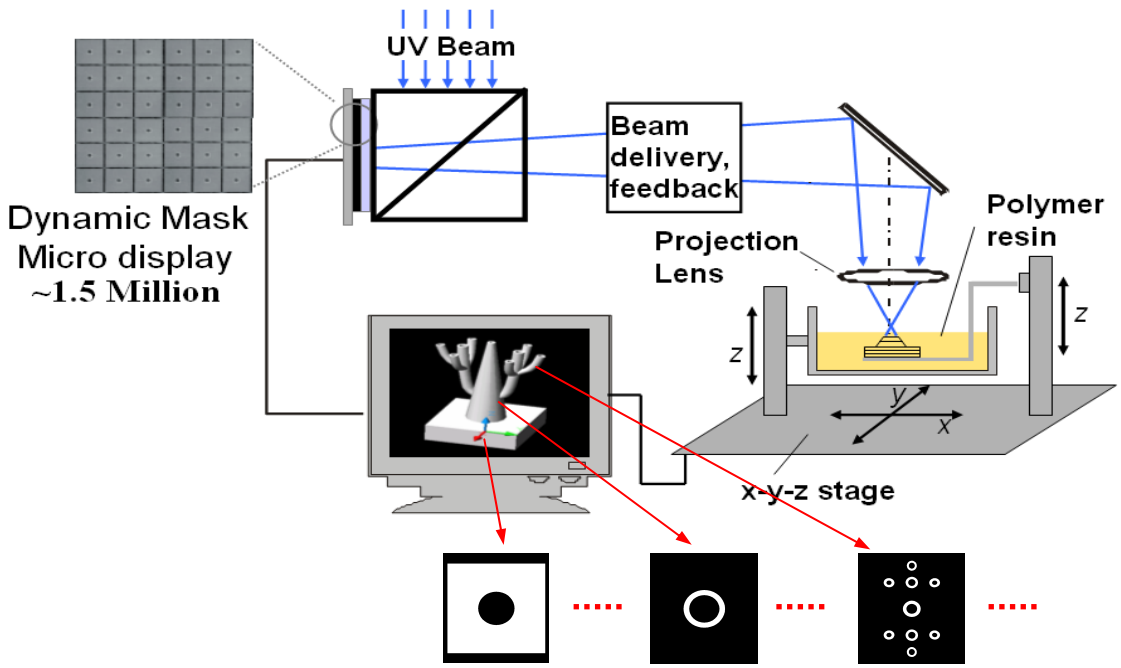

Fig. S1. **3D microfabrication by projection micro stereo-lithography.** 3D CAD drawing is sliced into a set of layers and the image of each layer is sent to a dynamic mask generator. Then, a light from flood UV source is reflected off the dynamic mask and the beam containing the image is focused on the surface of polymer resin through projection lens which reduces the image to the desired size. Once a layer is polymerized, stage drops the substrate by a predefined layer thickness, and the dynamic mask displays the next image for the polymerization of the next layer on top of the preceding one. This process proceeds iteratively until all the layers are complete.

Swelling ratio of hydrogel

Polymer specimen was fabricated to study equilibrium swelling ratio of the polymer in acetone (Fig. S2b). The specimen was polymerized under 6.74 mW cm^{-2} of UV (H-line, 436 nm). Exposure time for each layer is 12 seconds and thickness of each layer is 15 μm. The length of specimen was measured through microscope when it was dry and when it was in equilibrium swelling state in acetone (Fig. S2a). Swelling ratio was obtained by dividing the swollen length by the dry length. From the result shown in Fig. S2c, swelling ratio of the polymer under the fabrication condition described above is 1.42 ± 0.03. This value will change under different fabrication condition because of different cross-linking density of polymer.

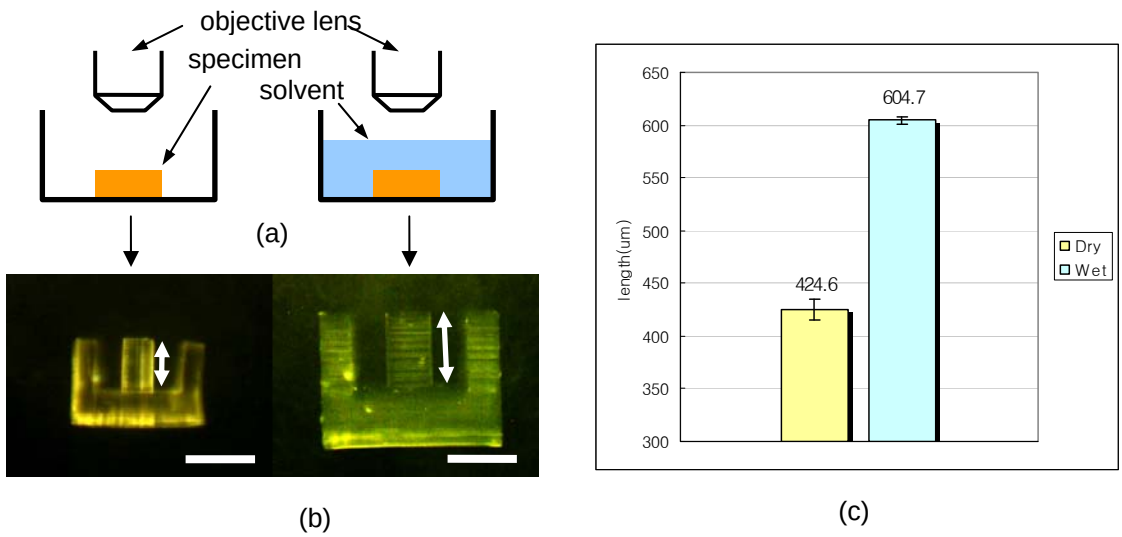

Fig. S2. Measurement of equilibrium swelling ratio. (a) Experimental setup to measure the length of the specimen. (b) Specimen when it is dry (left) and swollen (right). Scale bar indicates 500 μm. (c) Length of the specimen measured when it was dry and swollen. Swelling ratio (swollen length / dry length) from the data is 1.42 ± 0.03.

Diffusion-limited time scale of swelling actuation

We designed six cantilever beams with embedded microfluidic channel (Fig. S3a) in order to investigate the dependence of actuation timescale on diffusion length. All the beams are 1400 μm long and 200 μm wide. Channels are 150 μm × 50 μm in cross section, and embedded 25 μm from the

beam's outer surface. The dimension of the remaining part in the cross section where solvent needs to propagate through varies from 25 μm up to 275 μm with 50 μm increment (Fig. S3b). All the channels are filled with solvent immediately by capillary action when a droplet of solvent is applied to the opening of the channel at the base. As solvent diffuses into the walls of the channel, wet region swells while dry region remains unchanged. This causes the beams to bend. Since the ratio of swollen to dry region is different in each beam, timescale and deflection of bending motion is different. Note that beam 1 does not bend but extends only due to its symmetric cross section. In the video recorded from the front (Fig. S3c), the distance between the tip and the base of each beam was measured using image analysis software, and the bending angle (Fig. S3d) was calculated by assuming the shape of the curved beams is an arc. The actuation timescale decreases with the distance that solvent travels, which indicates that timescale of swelling actuation is determined by diffusion length. Also, the maximum bending of the beams decreases as the thickness of the beams increases. One of the reasons comes from the fact that the thicker the beams, the higher the bending rigidity. This result demonstrates that dimension of the actuator is a limiting factor for swelling actuation. Therefore, in swelling actuation without elastic instability, the dimension of the device needs to be smaller for faster actuation.

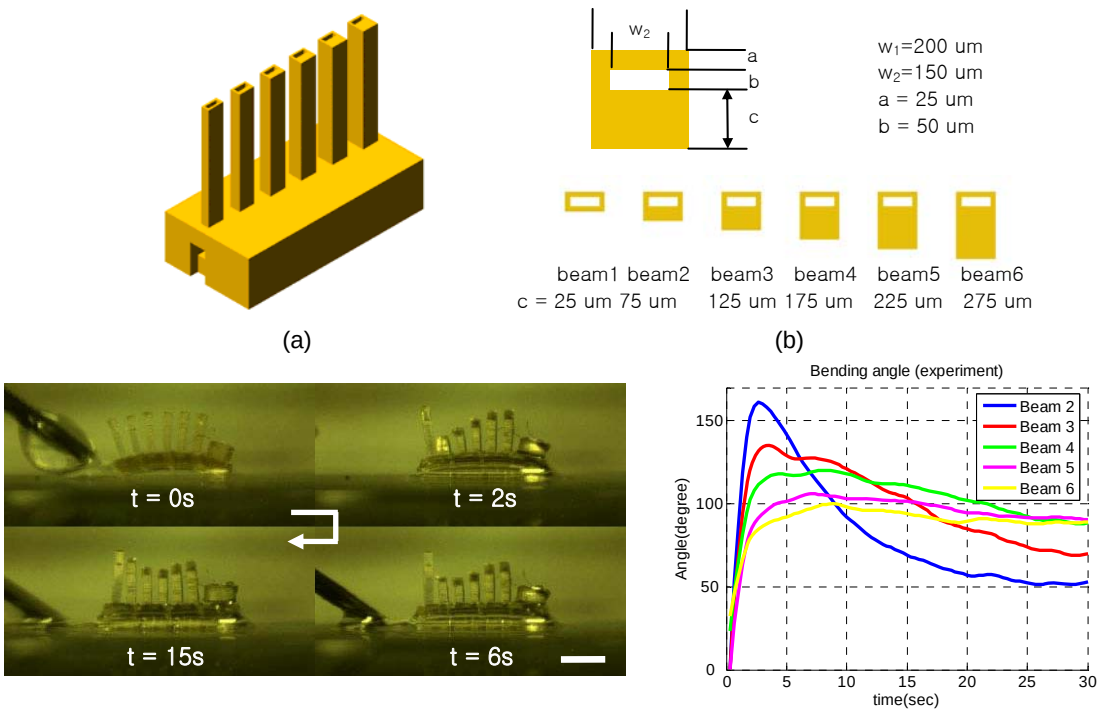

Fig. S3. Diffusion length as a limiting factor for actuation timescale. (a) Bending beams with embedded micro fluidic channels (beam height: 1400 μm, base: 2400 μm × 1200 μm). Channels are connected together in the base for simultaneous solvent delivery to all channels. (b) Cross sectional dimensions of each beam. (c) Motion of bending beams during swelling actuation. Scale bar indicates 1 mm. (d) Bending angle with time. No data for beam 1 because beam 1 does not bend but extends only due to its symmetric cross section.

Elastic instability of a doubly curved plate

Recent studies has unveiled the mysterious insect-trapping motion of Venus flytrap and found that secret is on the shape of their leaves; bending in doubly curved leaves gives rise to elastic instability which creates fast movement by snap-buckling. Following is a brief summary of theoretical basis of ref. 8 in the main text. Dimensionless total elastic energy of doubly curved plate due to bending and stretching deformation has been derived as

$$U(K_x, K_y; K_{xn}, \alpha) = U_{bending} + \alpha U_{stretching} = (K_x - K_{xn})^2 + (K_y - 1)^2 + \alpha(K_x K_y - 1)^2 \quad (1)$$

where $K_x = \kappa_x / \kappa$, $K_y = \kappa_y / \kappa$, and $K_{xn} = \kappa_{xn} / \kappa$ are dimensionless parameters representing the curvature in x direction, the curvature in y direction, and the natural curvature in x direction, respectively. The dimensionless geometric parameter $\alpha = L^4 \kappa^2 / h^2$ (L : radius of doubly curved plate, κ : initial curvature, h : thickness of doubly curved plate) determines the degree of coupling between bending and stretching energy. For a given α, the shape of the plate as a function of K_{xn} can be found by minimizing the total elastic energy U, i.e. solving the following equations.

$$\frac{\partial U}{\partial K_x} = \frac{\partial U}{\partial K_y} = 0 \quad (2)$$

Fig. S4a shows the solutions of equation (2) when $\alpha = 0, 0.5, 0.8, 1.0,$ and 1.5. We see that for α smaller than a critical value ($\alpha < 0.8$) the solution is unique, thus the shape of the shell changes continuously. On the other hand, for α greater than a critical value ($\alpha > 0.8$) there is a region in which multiple solutions exist. In this region, there is discontinuity in elastic energy between one

solution to the other as shown in Fig. S4b where the dimensionless elastic energy is plotted. The energy released from this energy gap is mostly converted into kinetic energy generating a rapid motion. This phenomenon becomes more apparent as the coupling parameter α increases.

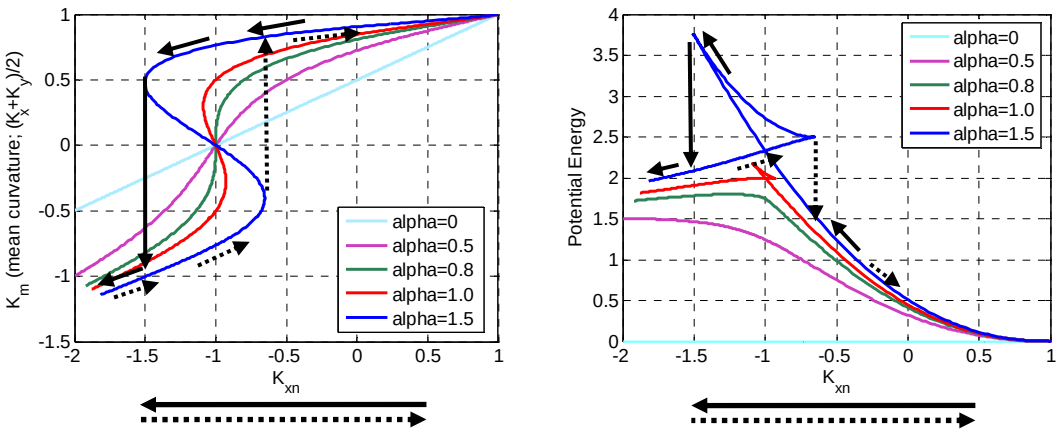

Fig. S4. Snap-buckling instability and energy release for rapid motion. (a) Geometric change with respect to natural curvature. Snap-buckling occurs for $\alpha \geq 0.8$. (b) Dimensionless energy change with respect to natural curvature.

Actuation speed enhancement – control experiment

The control sample was designed to demonstrate just uniaxial bending with the same structural resistance against swelling actuation as the doubly curved sample. This ensures that the motion of the control sample is same as the doubly curved device would do without elastic instability. The result shown in Fig. S5 tells that the doubly curved shape remarkably enhances the actuation speed of the device at the point of snap-buckling. The angle changed abruptly from 48˚ to 80˚ in 12 ms with a maximum angular velocity as high as 100 rad s^{-1}. On the contrary, in the control experiment, the angle change was slow and continuous with a maximum angular velocity less than 10 rad s^{-1}. Note that the angle change in doubly curved device is smaller before the snap-buckling point. This is another evidence that elastic energy is being stored in the structure before snap-buckling.

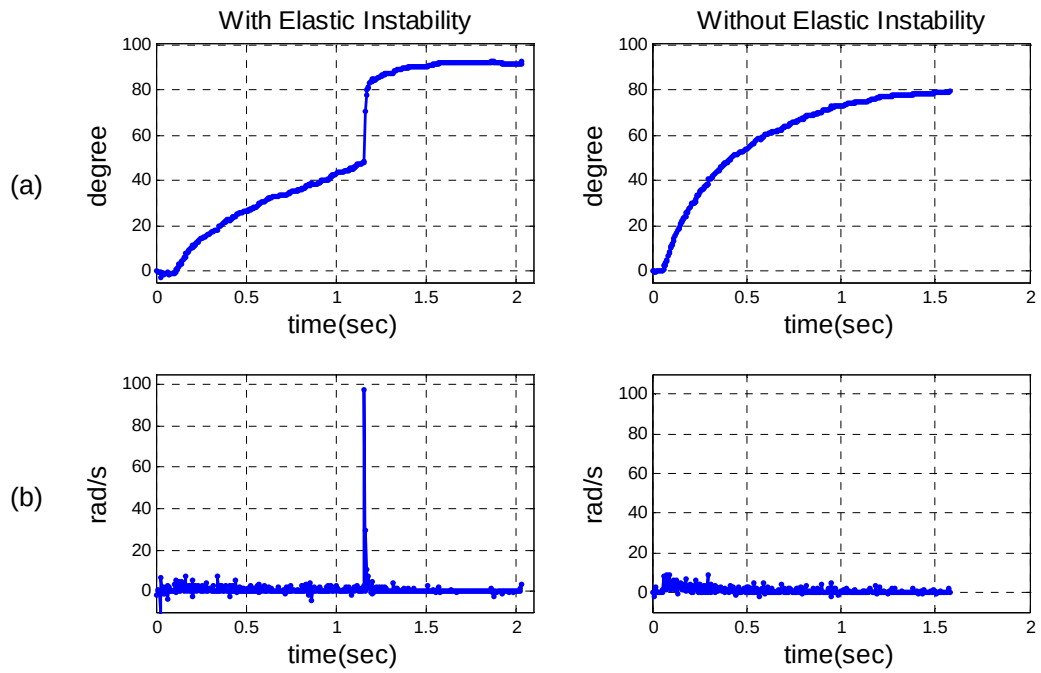

Fig. S5. Actuation speed enhancement by elastic instability (a) angular displacement and (b) angular velocity from actuators with (right column) and without (left column) elastic instability, respectively.

Effect of coupling parameter on snap-buckling

We fabricated two doubly-curved plates with different coupling parameters to investigate how the coupling parameter affects snap-buckling motion. Two samples have the same thickness h and length L, but different initial curvature κ, thus different dimensionless coupling parameter $\alpha = L^4\kappa^2/h^2$ (Table S1). Corresponding coupling parameter α of each sample is 3.5 and 6.2, respectively. For each device, the control sample was also fabricated to obtain the natural curvature κ_{xn} which would be the actual curvature without bending-stretching coupling. We captured the motion using high speed camera (Redlake Image, 125 fps) and extracted the curvature in vertical direction using circle fitting (Fig. S6a; κ_x in the left, κ_{xn} in the right in each Fig.). We analyzed every frame (125 fps) in the fast-moving range around the snap-buckling, but for the sake of efficiency

every fifth frame (25 fps) was analyzed in slow-moving range before and after snap-buckling. Fig. S6b shows the time course of the dimensionless curvature K_{xn} and K_x which are normalized with respect to the initial curvature. For both samples, the natural curvature K_{xn} changes smoothly, whereas at certain point the actual curvature K_x abruptly changed the sign from positive to negative, indicating the occurrence of snap-buckling. This is presented more effectively by plotting the actual curvature K_x against the natural curvature K_{xn} (Fig. S6c). The result that the slope of transition is steeper for the high coupling sample implies that the snap-buckling is more significant when α is greater. If it were not for the bending-stretching coupling ($\alpha = 0$), they would follow the dotted line on which the actual curvature K_x and the natural curvature K_{xn} are the same. Furthermore, it takes more time to trigger snap-buckling in high coupling sample (Fig. S6b, lower), which implies that as α increases more elastic energy needs to be stored owing to higher energy barrier. This suggests that for greater α more energy is released during snap-buckling, hence one can expect faster actuation. Ongoing experiments are investigating the actuation speed as a function of the coupling parameter.

Table S1. Dimension for two samples with different coupling parameters

	κ (μm^{-1})	t (μm)	L (μm)	α
low coupling	1/1150	63	370	3.5
high coupling	1/800	63	370	6.2

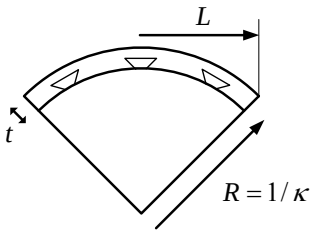

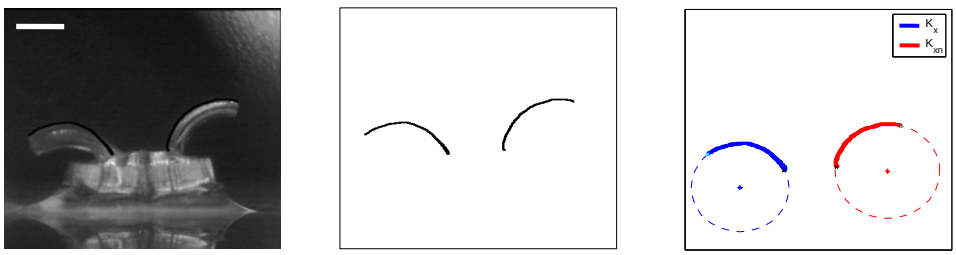

(a)

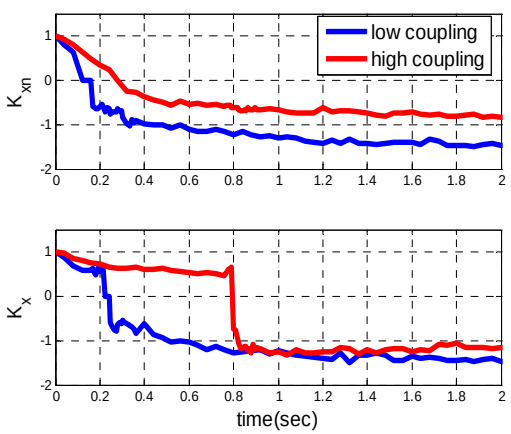

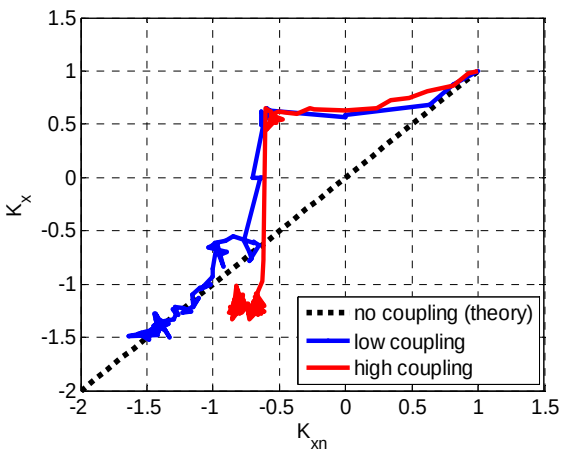

(b) (c)

Fig. S6. Coupling parameter and snap-buckling. (a) Data analysis to obtain the curvature of samples. For each frame of the video taken from the experiment, we drew lines along the curved surface and only these lines were extracted using image analysis software. Then curvature of these lines was calculated using circle fitting. (b) Dimensionless curvature change over time during experiment. (c) Actual curvature against natural curvature. The steeper the slope of transition (larger α), the more significant the snap-buckling is.

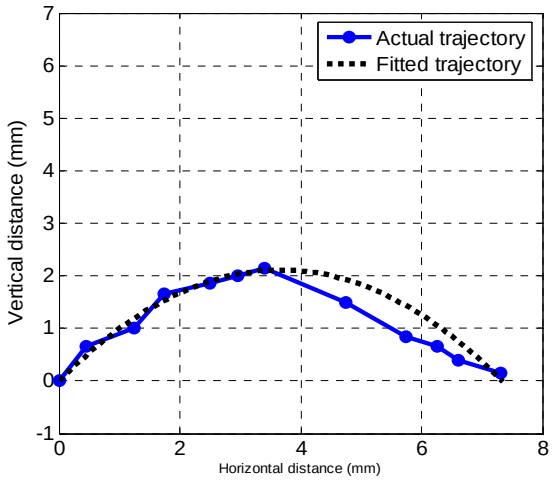

Fig. S7. Jumping trajectory for energy analysis. Trajectory of jumping motion is measured from experiment and fitted to an ideal parabola for estimation of energy release.

Movie 1. Snap-buckling of hydrogel actuator in doubly curved shape.

This movie shows real time motion of rapid actuation of micro hydrogel device in a doubly curved shape, followed by 5x slow motion. Snap-bucking occurs during swelling actuation, generating high angular velocity of 100 rad s^{-1} (Quick Time; 10 MB).

Movie 2. Control experiment with no elastic instability involved.

This movie shows real time motion of the control experiment, followed by 5x slow motion. Without elastic instability, the control sample experiences slow and continuous uniaxial bending with angular velocity of 10 rad s^{-1} (Quick Time; 10 MB).

Movie 3. Jump of micro hydrogel device.

This movie shows a real time jumping motion of microgel device. Two legs are doubly curved plates. Rapid actuation speed obtained by snap-buckling makes the device jump off the ground (Quick Time; 8 MB).